LIF thermometry with a sCMOS color camera and multiple dyes

C. Mucignat[1,*], T. Rösgen[2], I. Lunati[1]

1: Empa, Swiss Federal Laboratories for Materials Science and Technology, Laboratory of Computational Engineering, Dübendorf, Switzerland
2: Institute of Fluid Dynamics, Department of Mechanical and Process Engineering, ETH Zürich, Zürich, Switzerland
*Corresponding author: claudio.mucignat@empa.ch

Keywords:LIF, Color sCMOS, 2-dye.

ABSTRACT

We propose a method to perform accurate temperature measurements by means of Laser Induced Fluorescence (LIF). We use a sCMOS color camera and a 2-dye solution based on RuPhen, excited in the blue part of the visible spectrum. By changing the relative concentration of the dyes we can manipulate the color channels temperature sensitivity, which allows us to apply a laser power correction which is robust and less affected by image noise compared to convectional ratiometric approaches. Another advantage is that the overall temperature sensitivity is only partially reduces compared to the one of RuPhen, which is not the case if a ratiometric approach is chosen. The method is demonstrated on a bench-top setup, where temperatures can be precisely controlled. An error analysis shows that an accuracy better than $0.5°C$ is possible. The correction method can be applied to other measurement techniques, such as Pressure Sensitive Paints (PSPs).

1. Introduction

Given their ability to enhance our comprehension of the coupled heat and momentum transfer in thermal fluid flow applications, many studies have concentrated on non-intrusive measurement techniques that quantify temperature fields in experimental fluid dynamics (see, e.g., (Yarin et al., 2007; Tagawa et al., 2001; Lavieille et al., 2000; Fujisawa et al., 2005)). In this regard, Laser Induced Fluorescence (LIF, Walker (1987); Coppeta & Rogers (1998)) is a cutting-edge, whole-field non-intrusive technique that employs temperature-dependent fluorescence to convert emission intensity into temperature. For this purpose, the choice of the illumination source and the dye(s) is crucial for the sensitivity and accuracy of the measurement. For example, the use of a second dye can allow a reduction of the experimental uncertainties. In this case the use of a ratiometric approach, employed for instance also in pressure sensitive paint methods (see Barigozzi et al. (2018)), allows to compensate non-uniform laser power fluctuations. However, this comes with additional requirements for the choice of the dyes Coppeta & Rogers (1998), which should have a

common excitation band but separate emission bands. It is also necessary to record intensity images at separating the emission of the dyes by using bandpass filters and multiple cameras, which often reduces the signal-to-noise (SNR) ratio. The resulting sensitivity with respect to temperature is typically less $2\,\%/^{\circ}\mathrm{C}$ and can be lower compared to that of the single dyes, thus reducing the quality of the data. For example, Rochlitz & Scholz (2018) proposed a 2-dye technique using a pulsed 532 nm laser, two monochrome cameras with band-pass filters with as Rhodamine B and Rhodamine 110 as the dyes. The temperature sensitivity was found to be $1.7\,\%/^{\circ}\mathrm{C}$. Another study employed two non-toxic dyes (fluorescein, chlorophyll) to perform ratiometric two color-two dye (2c/2d) LIF along with Particle Image Velocimetry (PIV) measurements (Shah et al. (2018)). As in Rochlitz & Scholz (2018) , the experimental setup exhibited considerable complexity due to the use of a pulsed Nd:YAG laser and a minimum of three monochrome cameras (two for 2c/2d ratiometric LIF and one for PIV). This configuration required a pixel-to-pixel mapping of the recordings of all three cameras, as well as the use of beam-splitter optics to separate the fluorescence signals, thereby reducing the signal-to-noise ratio. A further limitation was the low absorption of fluorescein at $532\,\mathrm{nm}$, which required a higher concentration of the dye and higher laser energies for single-shot temperature measurements. In order to reduce the experimental complexity, one study has attempted to simultaneously quantify the velocity and temperature fields in aqueous flows by means of an Ar-ion laser (λ_e = $488\,\mathrm{nm}$), a color CCD camera, $7\,\mu\mathrm{m}$ particles, and a two-color/two-dye (2c/2d) combination of RhB/Rh110 Funatani et al. (2004). To obtain the temperature field in a buoyant plume, the ratio of red/green channels and tracer displacement in the blue channel were used. The temperature sensitivity of the fluorescence signal was found to be $1.7\,\%/^{\circ}\mathrm{C}$ and the temperature field was prone to errors due to the overlap between the Bayer filter characteristics and the emission spectra of the two dyes.

In our previous work (Shah et al., 2024) we proposed a simultaneous approach to perform PIV and LIF using a single color camera and a single laser source. In this work we used a novel dye, namely RuPhen (Lam et al. (2012)), which showed an excellent sensitivity (up to $4\,\%/^{\circ}\mathrm{C}$) and has emission spectrum which overlaps almost perfectly with the peak quantum efficiency of camera red channel (i.e. $550\,\mathrm{nm}$–$770\,\mathrm{nm}$) and peak absorption at $470\,\mathrm{nm}$. Here we extend the technique by adding a second dye to to increase the calibration accuracy, thus enabling a robust laser power fluctuation correction.

2. Methods

2.1. Camera

We use a high-sensitivity sCMOS color camera, the PCO edge 5.5. The camera has a raw resolution of 2560×2160 px with an 'rggb' Bayer filter pattern. The quantum efficiencies of the camera in the different color channels are shown in Fig. 2 (red, green and blue lines), along with the absorption and emission spectra of fluorescein. According to the manufacturer the non-linearity of the camera is below 0.6%.

2.2. Setup

A cuvette with sample solutions is placed in a temperature-controlled enclosure. We monitor the temperature by means of calibrated type K thermocouples. The sensors have a cold junction compensation, allowing for an accuracy of 100 mK. The solution is excited by means of a high-power LED light (VOLPI Intraled 2020), which was modified by adding a Peltier cooler to increase the stability of the illumination power, found to be within 1%. A bandpass filter (CWL $450\ 10nm$ FWHM) is used to obtain an excitation band similar to a CW blue laser. Furthermore, we employ an hot mirror to avoid heating of the sample due to IR radiation emitted from the lamp.

2.3. Spectromter

To identify a suitable mixture dye, we measure the absorption and emission spectra of several combinations of a Ruthenium-based dye, RuPhen (Tris(1,10-phenanthroline)ruthenium(II) chloride hydrate, CAS No. 207802-45-7), with a second fluorescent dye using a compact spectrometer (Thorlabs CCS200/M).

2.4. Calibration model

We model the fluorescence emission of the mixtures with a single (Eq.2) or double exponential model (Eq. 4). Note that we in Eq. (2) we also report the inverse models, where the superscripts 1 and 2 denote a calculated temperature using a single or a double exponential model, respectively. The models have to be verified for various combinations of dyes and concentrations. In Eq. (2) and Eq. (4) R_n and G_n correspond to the intensity of the red and green channel normalized by a reference. We remark that normalization allows for the correction of the absorption effects.

$$R_n(T) = \Gamma\alpha_R\, e^{-\beta_R T}\ , \qquad T_1(R_n) = -log(\frac{R_n}{\Gamma\alpha_R})/\beta_R \tag{1}$$

$$G_n(T) = \Gamma\alpha_G\, e^{-\beta_G T}\ , \qquad T_1(G_n) = -log(\frac{G_n}{\Gamma\alpha_G})/\beta_G \tag{2}$$

$$R_n(T) = \Gamma\alpha_R\, e^{-\beta_R T_R^{\lambda}}\ , \qquad T_2(R_n) = (-log(\frac{R_n}{\Gamma\alpha_R})/\beta_R)^{1/\lambda_R} \tag{3}$$

$$G_n(T) = \Gamma\alpha_G\, e^{-\beta_G T_G^{\lambda}}\ , \qquad T_2(G_n) = (-log(\frac{G_n}{\Gamma\alpha_G})/\beta_G)^{1/\lambda_G} \tag{4}$$

Note that Γ is a correction factor for laser power fluctuations, as outlined in the next section. We fit the calibration model using a weighted nonlinear least-squares method employing the Effective Variance (Tellinghuisen, 2020).

2.5. Laser Power fluctuation correction

We follow the same approach as in Shah et al. (2024). Briefly, instead of exploiting the ratiometric approach we leverage the assumption that the temperature obtained by using R_n and G_n must be locally the same. If not a correction factor Γ can be calculated based on the mismatch. For the sake of conciseness we refer the reader to our original work (Shah et al. (2024)), while here we report the solutions for Γ applying the two calibration models. In particular, if the single exponential model, there is an explicit solution that reads:

$$log(\Gamma) = \frac{\beta_R \beta_G}{\beta_R - \beta_G}(T_R - T_G) \tag{5}$$

Note that in Eq. (8), T_R and T_G denote the temperatures derived without laser power correction, with $\Gamma = 1$. On the contrary, for the double exponential model (Eq. (4)) there is not an explicit solution and a minimization problem has to be solved globally or for a sub-domain of R and G pixels:

$$\left[(log(\frac{R_n}{\Gamma\alpha_R})/\beta_R)^{1/\lambda_R} - (log(\frac{G_n}{\Gamma\alpha_G})/\beta_G)^{1/\lambda_G}\right] \rightarrow min \tag{6}$$

Note that the estimate for Γ is independent of the actual local intensity and temperature. Thus, averaging over neighboring RGB pixels can be performed to improve the estimate.

In the case of the single exponential model one can perform an error analysis based on standard error propagation. The temperature correction based on T_R and T_G reads:

$$T_C = T_R + \frac{log\Gamma}{\beta_R} \tag{7}$$

with

$$log\Gamma = \frac{\beta_R \beta_G}{\beta_R - \beta_G}(T_R - T_G) \tag{8}$$

Thereafter, T_C can be rewritten as:

$$T_C = T_R + \frac{\beta_R \beta_G}{\beta_R - \beta_G}(T_R - T_G)\frac{1}{\beta_R} \tag{9}$$

or

$$T_C = \frac{\beta_R}{\beta_R - \beta_G}T_R - \frac{\beta_G}{\beta_R - \beta_G}T_G \tag{10}$$

The partial derivatives of T_C with respect to T_R and T_C are

$$\frac{\partial T_C}{\partial T_R} = \frac{\beta_R}{\beta_R - \beta_G} \tag{11}$$

$$\frac{\partial T_C}{\partial T_G} = -\frac{\beta_G}{\beta_G - \beta_G} \tag{12}$$

So using the standard error propagation we get

$$\frac{\delta T_C}{T_C} = \frac{\beta_R - \beta_G}{\beta_R T_R - \beta_G T_G} \sqrt{\left(\frac{\beta_R}{\beta_R - \beta_G}\right)^2 \delta T_R^2 + \left(\frac{\beta_G}{\beta_R - \beta_G}\right)^2 \delta T_G^2} \tag{13}$$

or

$$\frac{\delta T_C}{T_C} = \sqrt{\frac{\beta_R^2 \delta T_R^2 + \beta_G^2 \delta T_G^2}{(\beta_R T_R - \beta_G T_G)^2}} \tag{14}$$

The equation above allows us to study the effects of $\beta_{R,G}$ and δ_{T_C,T_G} at varying $T_{R,G}$ under the assumption of a single exponential model(Eq. (2)). What is missing is an estimate for δT_R and δT_G. These can be estimated by multivariate Monte-Carlo regression, where setting confidence intervals for In and T, for which we assume $\sigma_I = 0.01\ \%$ and $\sigma_T = 0.1\ K$. Typical values for ϵ_{95} are in the order of $0.2 - 0.3\ K$ for T_R and T_G if a confidence level of 95% is chosen, while for the corrected temperature we have $\epsilon_{95} = 0.5\ K$.

3. Results

3.1. Dye selection

First, we characterise the emission and absorption spectra at varying sample temperatures for single dye solutions and compare them with the quantum efficiency curves of the color camera. Besides fluorescein (Fig. 2) we also test natural dyes such as vitamins proposed by Zähringer (2014). In this context, Riboflavin (Fig. 3) is interesting as its absorption and emission spectra show a fairly large Stokes shift and it has a very good overlap with the quantum efficiency of the green channel Fig. 3. On the contrary, fluorescein has the least separation between emission and absorption (Fig. 2), which could lead to "type 1 errors" (see the work from Coppeta and Rogers Coppeta & Rogers (1998)). All dyes show a very low sensitivity of absorption to temperature (Fig. 1,Fig. 2,Fig. 3).

Next, we consider adding to a RuPhen solution a small amount of fluorescein which has very small temperature sensitivity when excited below 490 nm and high quantum yield (Fig. 2). The key is to find the proper relative concentration of Rupen and fluorescein to avoid that the emission of the latter dominates, thus reducing the temperature sensitivity (see section Section 3.2). We also measure absorption and emission of a mixture containing a small concentration of Riboflavine (0.04mg/l) and 0.17mg/l of RuPhen. Both mixtures have a an absorption spectra which is dominated by RuPhen. On the contrary in the green spectrum (i.e. $500\,\mathrm{nm}$–$550\,\mathrm{nm}$) the effect of the second dye is evident, reducing the local sensitivity to the temperature.

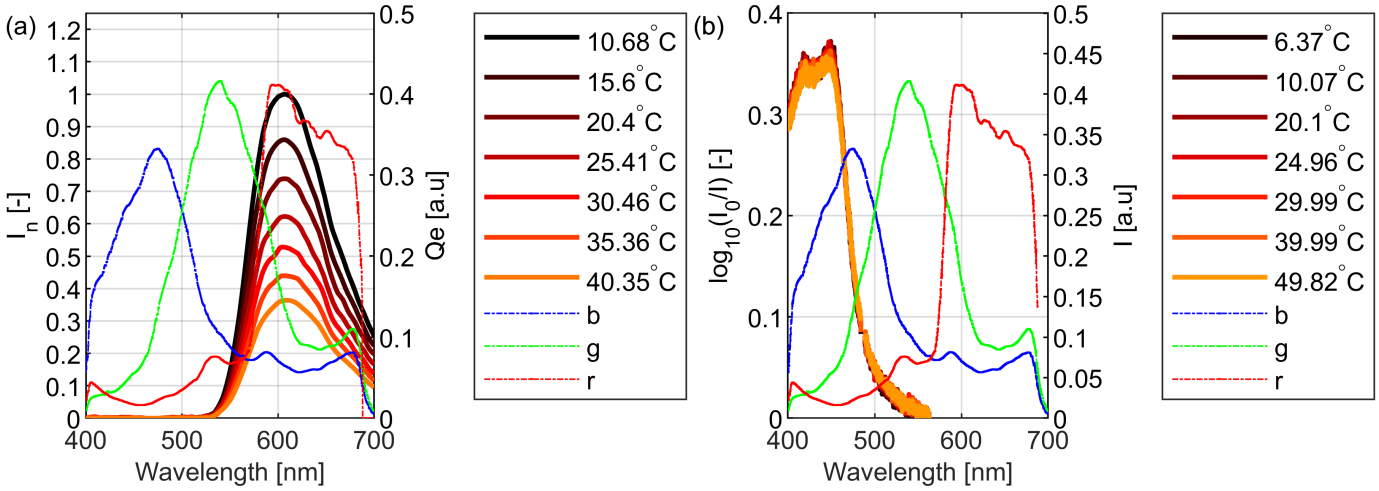

Figure 1. Emission (a) and absorption (b) of RuPhen (16mg/l) at different temperatures and PCO edge QE curves.

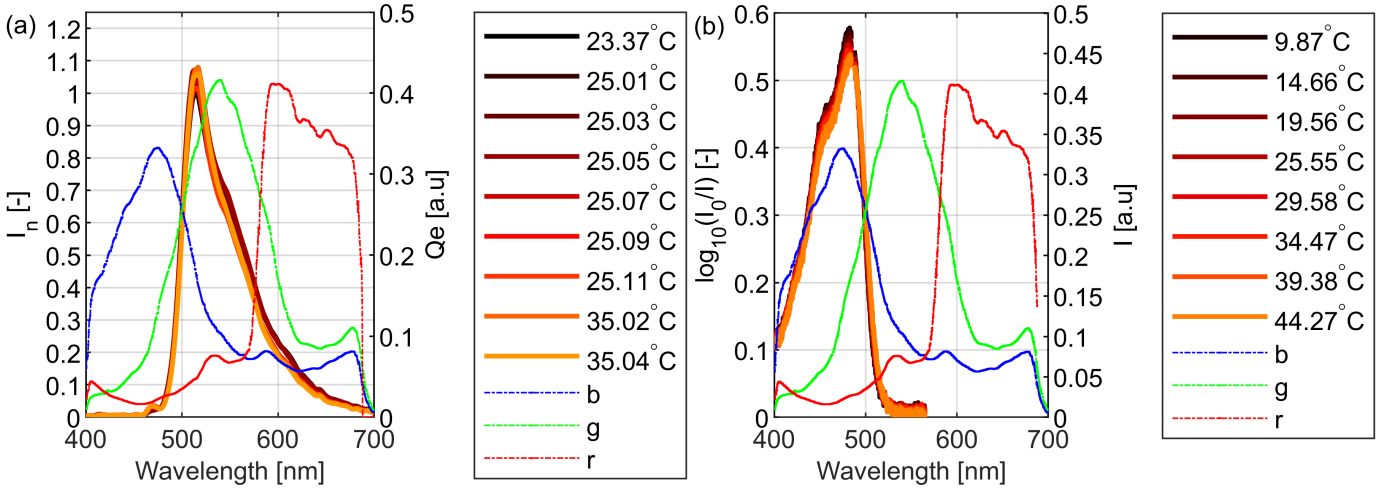

Figure 2. Emission (a) and absorption (b) of Fl (0.8mg/l) at different temperatures and PCO edge QE curves.

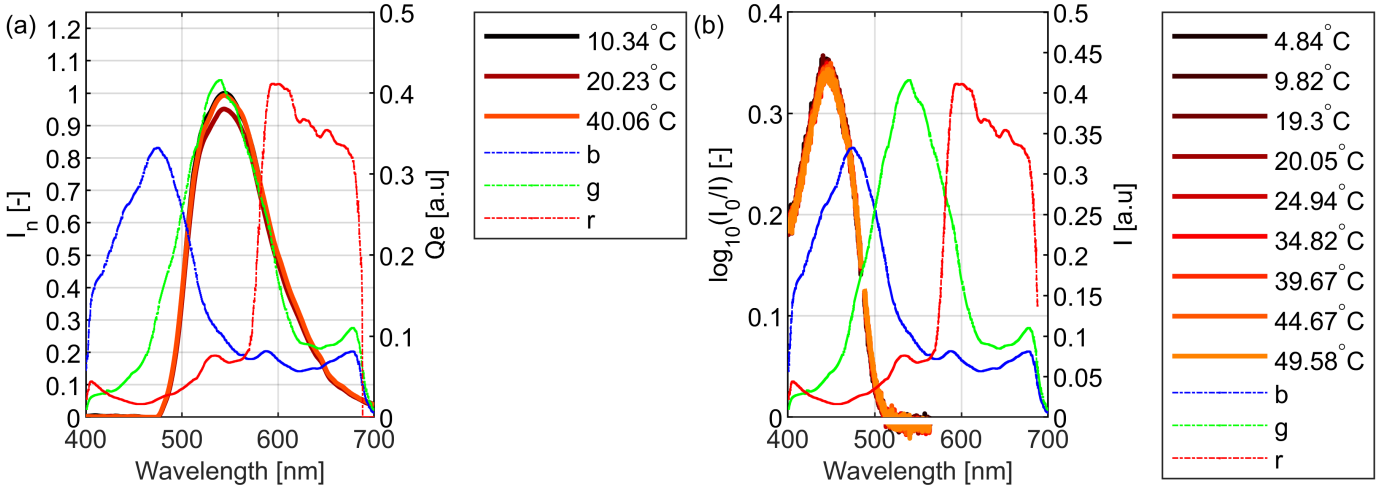

Figure 3. Emission (a) and absorption (b) of Riboflavin at different temperatures and PCO edge QE curves.

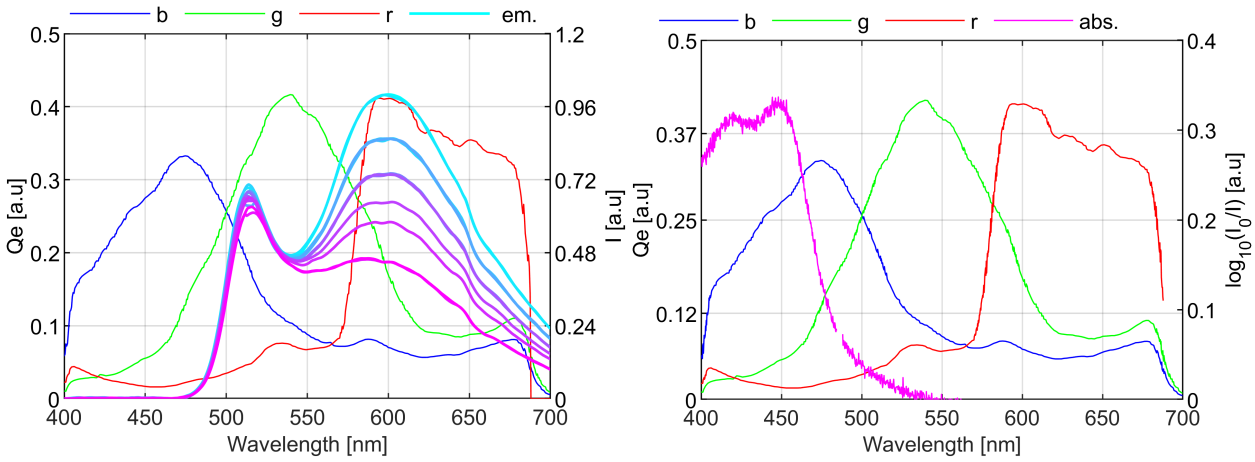

Figure 4. Emission and absorption of Fl (0.03mg/l) and RuPhen (16mg/l) at different temperatures.

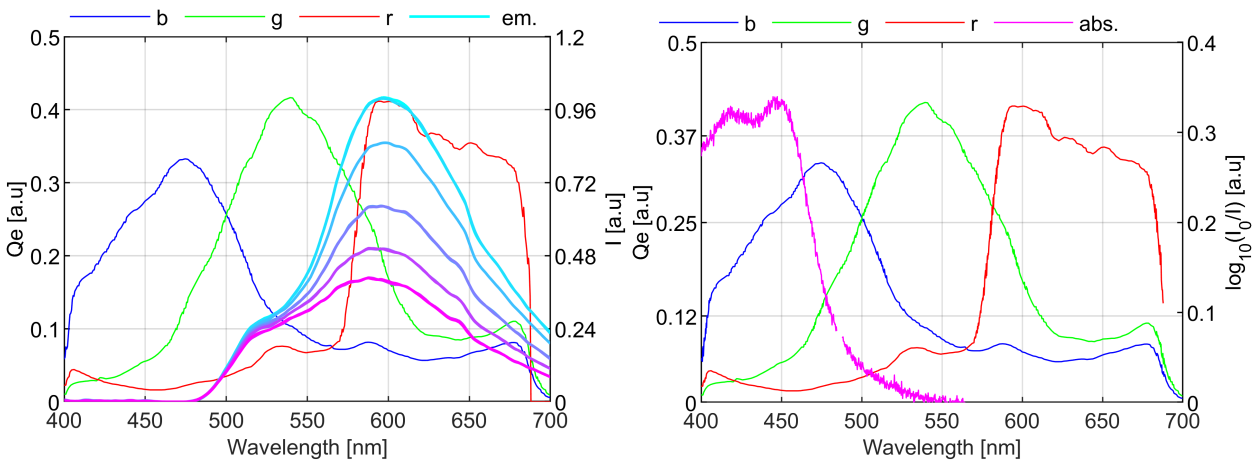

Figure 5. Emission of Riboflavin (0.04mg/l) and RuPhen (0.17mg/l) at different temperatures.

3.2. Calibration with spectrometer data

We test the models in Eq. (2) and Eq. (4) using the emission spectra measured by the spectrometer, by multiplying them with the quantum efficiency curves of the color camera and integrating the resulting intensity, allowing us to mimic the response of the color camera. In this specific case we consider three different mixtures with a constant concentration of Ruhpen (17 mg/l) and increasing concentration of fluorescein (0.013, 0.026 and 0.036 mg/l). Fig. 6-Fig. 8 show that the sensitivity coefficient (namely α in Eq. (2)), of both R and G channels decreases with the relative concentration of fluorescein. Notably, the concentration of the latter is O^{-3} smaller than the one of RuPhen (see Table 1), due to its significantly higher quantum yield. Moreover, the plots show that the double exponential model is capable of reaching a lower mean fit error, ϵ, suggesting that it may allow for a higher precision.

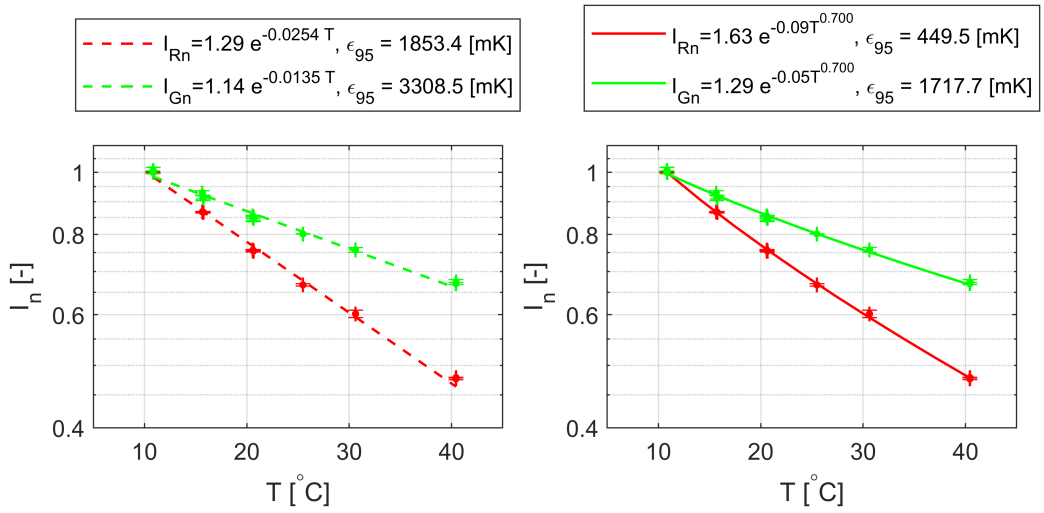

Figure 6. Spectrometer data. Calibration curves for a solution with 17 mg/l of RuPhen and 0.036 mg/l fluorescein. The legend show the coeffcient of the models and the the calibration residual with 95% confidence level ϵ_{95}

.

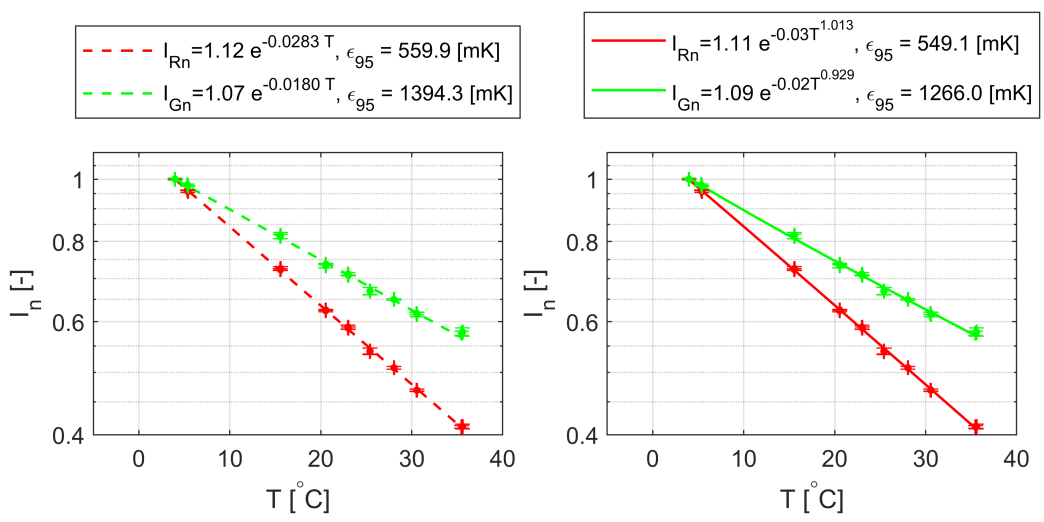

Figure 7. Spectrometer data. Calibration curves for a solution with 17 mg/l of RuPhen and 0.026 mg/l fluorescein. The legend show the coeffcient of the models and the the calibration residual with 95% confidence level ϵ_{95}

.

C_{RuPhen} [mg/l]	$C_{fluorescein}$ [mg/l]	$C_{fluorescein}/C_{RuPhen}$ [%]	$\lvert\beta_R\rvert$ [%/°C]	$\lvert\beta_G\rvert$ [%/°C]
16.55	0.013	0.08	3.1	2.5
16.00	0.026	0.17	2.8	1.8
17.42	0.036	0.21	2.6	1.4

Table 1. Red and Green channel sensitivities using the single exponential model (Eq. (2)) for different relative concentrations of RuPhen and fluorescein.

3.3. Color camera data - calibration

We perform a calibration using a mixture of fluorescein and RuPhen using the same setup but recording the LIF signal with the color camera. For each temperature we record 20 images with

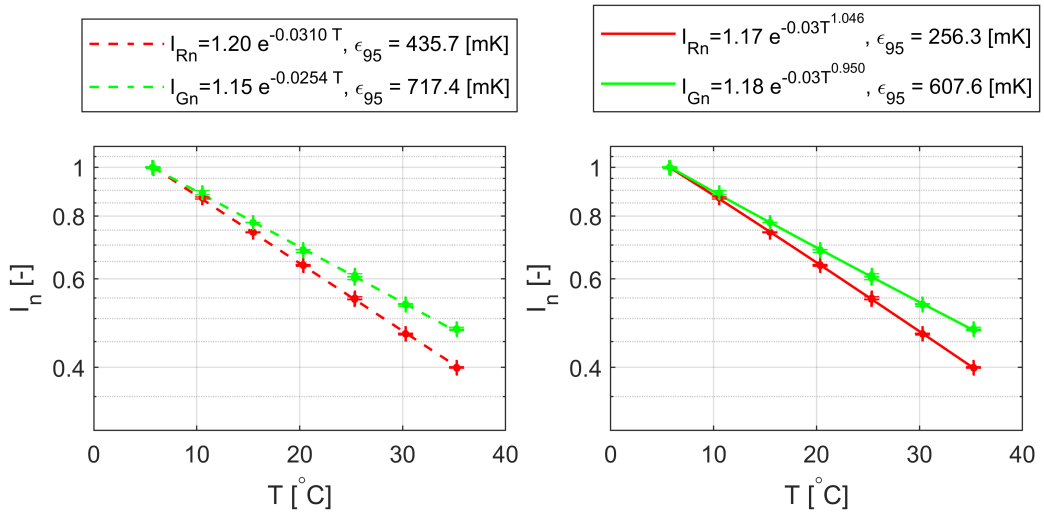

Figure 8. Spectrometer data. Calibration curves for a solution with 17 mg/l of RuPhen and 0.013 mg/l fluorescein. The legend show the coeffcient of the models and the the calibration residual with 95% confidence level ϵ_{95}.

an exposure time of 100 ms and average them together (a sample recording is shown in Fig. 9, left panel). To increase the SNR, we apply a 4×4 binning, summing the intensity values. Subsequently, normalized intensity maps are obtained by subtracting the dark image and dividing by a reference intensity map, chosen as the recording at the lowest temperature. Next we take the median value and fit the calibration coefficients for Eq. (2) and Eq. (4). For comparison, we also perform a calibration following classic ratiometric approaches, where we use normalized intensities defined as $I_{R,G} = R_n/G_N$.

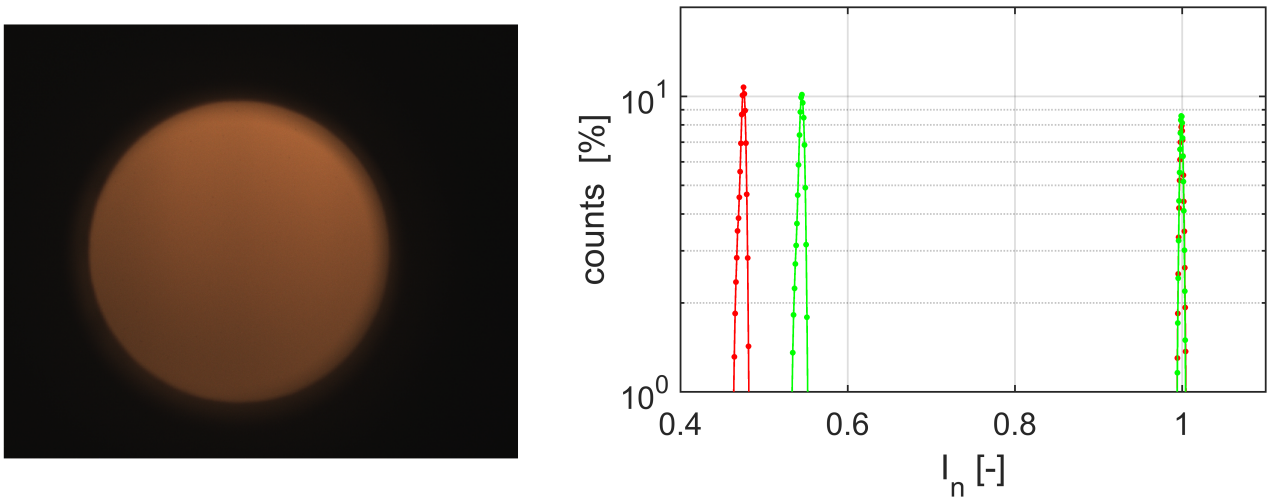

Figure 9. Left panel: Raw image recorded at 20.20 $°C$. Right panel: Histograms of the normalized intensity for R, G and B channels for two recordings at $T = 12.1°C$ and at $T = 20.1°C$.

Before proceeding to the calibration results, the right panel in Fig. 9 shows the histograms of R_N,G_N, and B_N for two recordings, one at $T = 10.2°C$ and one at $T = 35.1°C$. The data allows us to observe that the images have a very uniform intensity distribution with low standard deviation (denoted as σ). Indeed the distribution of both R_n and G_n have 3σ intervals below 0.01.

This is crucial to ensure that temperature non-uniformity effects (for due instance to stratification or convection) are negligible and do not affect the calibration curves.

Next, we report in Fig. 10 the resulting calibration curves obtained using the single and double exponential models. While for both ϵ_{95} is below 0.5 K, the double exponential is able to better fit the calibration data on both red and green channels. This observation is supported by Fig. 10

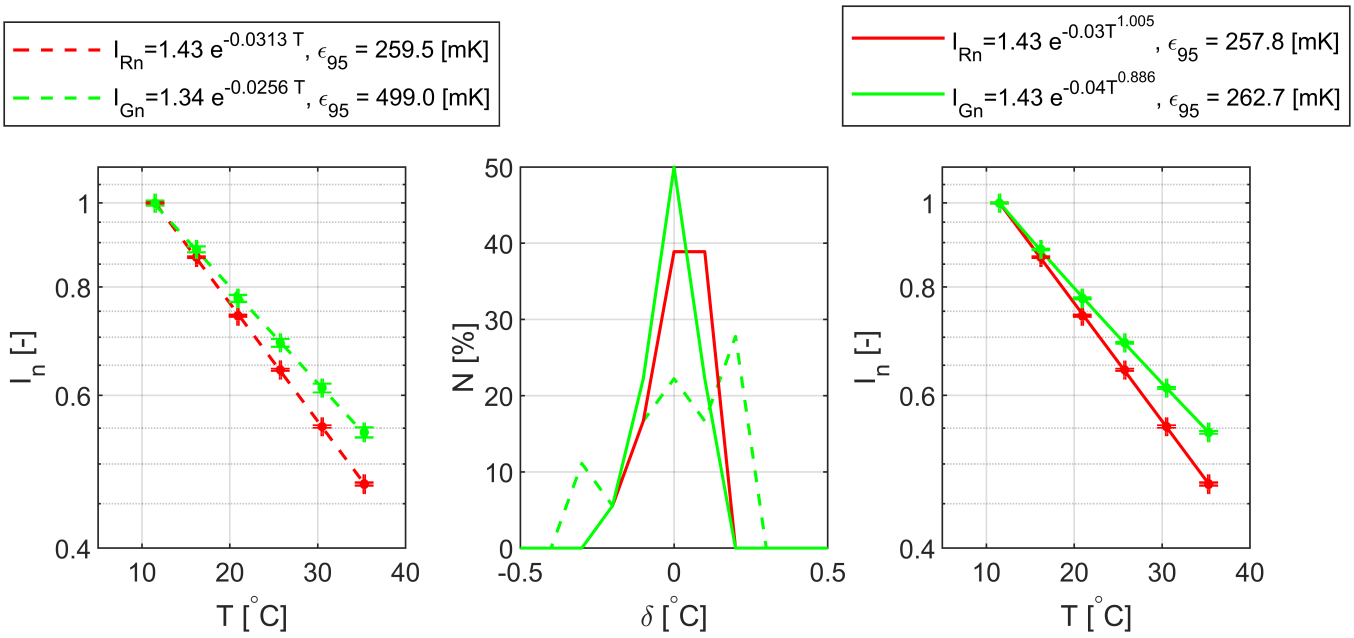

Figure 10. Left panel: Markers show the measured I_R and I_G, dashed lines report the calibration curves according to Eq. (2). Middle panel: histogram of the fit error ϵ for single and double exponential models. Right panel: Markers show the measured I_R and I_G, continuous lines report the calibration curves according to Eq. (4).

(mid panel) where we report the histogram of ϵ, showing that the double exponential model has a distribution centered at 0, while the other model is affected by a small non-linear bias. For this specific solution we report a sensitivity of the red channel equal to $3\%/°C$ and $2.4\%/°C$ for the green one. For completeness, Fig. 11 reports the calibration data and the residual calibration error following a ratiometric approach. Again, Eq. (4) allows for lower errors, while Eq. (2) is affected by high non-linear bias. In this case, the resulting sensitivity is considerably lower, i.e. $0.6\%/°C$.

3.4. Color camera data - test

We perform an experiment, setting a sample temperature to about 18.4 and 27.9 $°C$ and we record 20 images setting the LED illumination power to -30,-10, 0, and +10 $\%$ of the nominal value used during calibration. Note that the set temperature does not correspond to a value used for calibrating the system. The top panel in Fig. 12 reports the histograms of the maps of $T_2(I_R)$ and $T_2(I_G)$ obtained by varying the illumination power for a sample temperature of 18.4 $°C$. As expected, using just the red or green channel does not allow for a correct measurement, yielding to large errors. On the contrary (Fig. 12 bottom panel) the laser power correction proposed in this

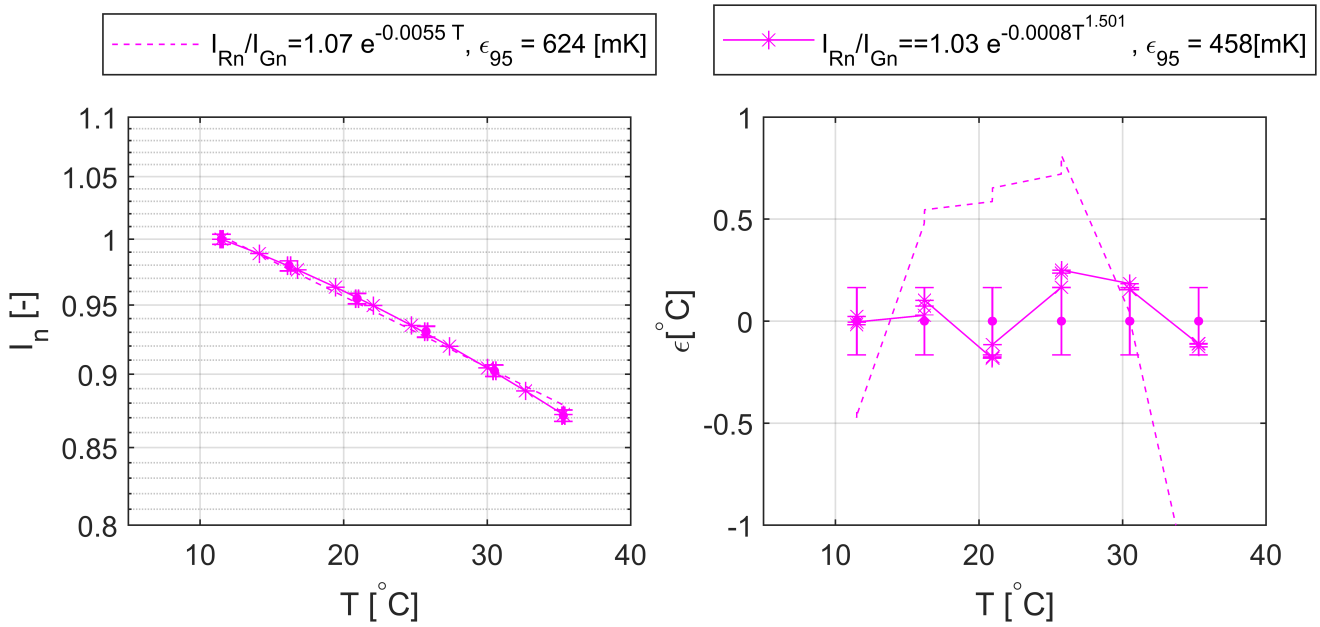

Figure 11. Left panel: Markers show the measured ration I_R/I_G, dashed lines report the calibration curves according to Eq. (2). Right panel: Markers show the measured ratio I_R/I_G, continuous lines report the calibration curves according to Eq. (4).

work and in Shah et al. (2024), allows to reduce the experimental errors considerably. Upon closer examination, between $T_2(I_R\Gamma)$ and $T_1(I_R\Gamma)$, the former provides better precision relative to the measured sample temperatures (indicated in both panels with black dashed lines). Additionally, we have included the histograms of $T_2(I_R/I_G)$, derived using a traditional ratiometric method. This demonstrates that while the ratiometric method can correct for laser power fluctuations, its lower sensitivity results in histograms with a standard deviation up to three times larger. Table 2 reports the mean values and the 3σ interval for each calculated temperature, showing that the proposed laser power correction method, coupled with a 2 dye approach, allows for a reduction of the random errors (i.e. lower standard deviation of the calculated temperature maps) while retaining a good precision in estimated the sample temperature measured by the thermocouples.

I_{LED} [%]	T_S [$^\circ C$]	$T_2(I_R)$ [$^\circ C$]	$T_1(I_R/\Gamma)$ [$^\circ C$]	$T_2(I_R/\Gamma)$ [$^\circ C$]	$T_2(I_R/I_G)$ [$^\circ C$]
-30	18.4	28.9, $3\sigma = 0.5$	17.4 , $3\sigma = 0.5$	18.3 , $3\sigma = 0.5$	17.6 , $3\sigma = 2.1$
-10	18.4	21.2, $3\sigma = 0.4$	17.6 , $3\sigma = 0.4$	18.5 , $3\sigma = 0.4$	17.8 , $3\sigma = 1.8$
0	18.4	18.4, $3\sigma = 0.4$	17.7 , $3\sigma = 0.4$	18.5 , $3\sigma = 0.4$	17.9 , $3\sigma = 1.8$
+10	18.4	15.9, $3\sigma = 0.55$	17.7 , $3\sigma = 0.4$	18.6 , $3\sigma = 0.4$	17.9 , $3\sigma = 1.7$
-30	27.9	38.4, $3\sigma = 0.7$	27.5 , $3\sigma = 0.7$	27.8 , $3\sigma = 0.7$	27.6 , $3\sigma = 2.0$
-10	27.9	30.6, $3\sigma = 0.6$	27.4 , $3\sigma = 0.6$	27.7 , $3\sigma = 0.6$	27.8 , $3\sigma = 1.8$
0	27.9	27.8, $3\sigma = 0.6$	27.5 , $3\sigma = 0.6$	27.8 , $3\sigma = 0.6$	27.9 , $3\sigma = 1.7$
10	27.9	25.3, $3\sigma = 0.5$	27.5 , $3\sigma = 0.5$	27.8 , $3\sigma = 0.5$	27.9 , $3\sigma = 1.7$

Table 2. Sample and calculated temperatures at varying illumination power.

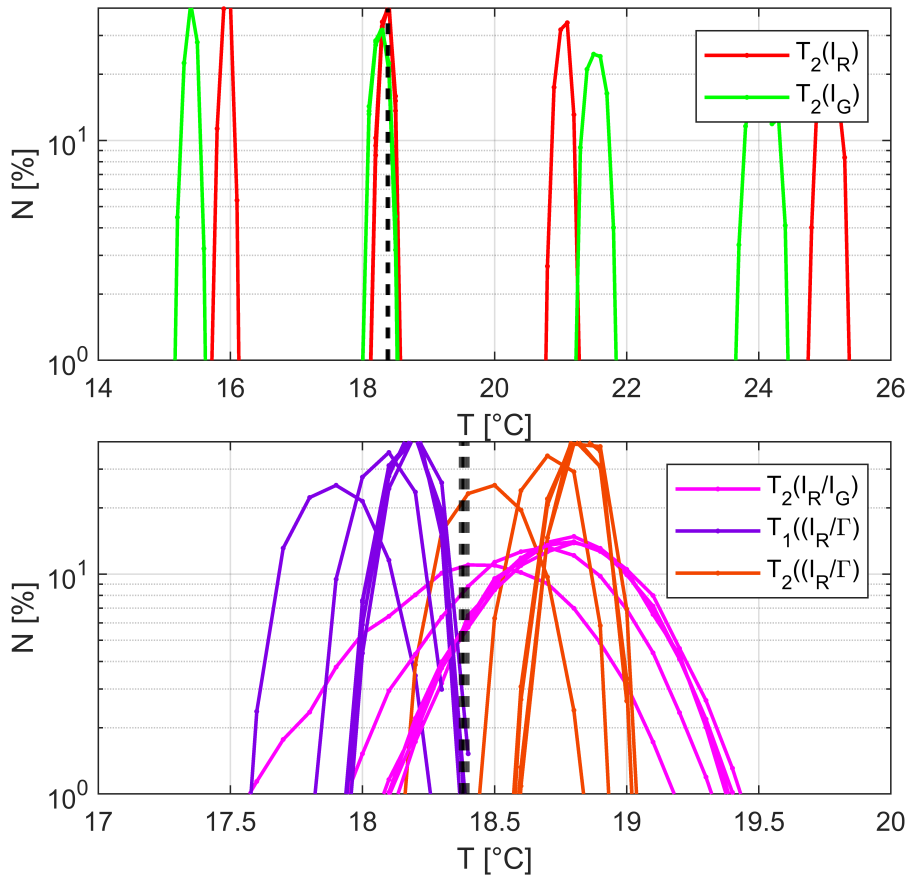

Figure 12. Top panel: histograms of $T_2(I_R)$ and $T_2(I_G)$ setting the LED illumination power to -30,-10, 0, and +10 % of the nominal value; black lines report the measured cuvette temperature. Bottom panel: histograms of $T_2(I_R/I_G)$, $T_1(I_R/\Gamma)$ and , $T_2(I_R/\Gamma)$ setting the LED illumination power to -30,-10, 0, and +10 % of the nominal value; black lines report the measured cuvette temperature.

3.5. Color camera data - error analysis

Finally, we use the Eq. (14) to perform error analysis for the data shown in Section 3.4. Note that that this is a simplified approach by referring to a single exponential model, as λ_R and λ_G in the case of a double exponential model are close to 1. Fig. 13 shows the relative and absolute error maps for various combinations of β_R and β_G. Here, we assume $k = 20$, $\epsilon_{95} 0.5K$ for T_R and T_G, and that the calculated T_R and T_G are equal to 18 and 16 $°C$ respectively. The plot indicates with a white cross the actual values of β_R and β_G derived after calibration (see Fig. 10). For these specific values, the error on the corrected temperature is below 0.5 K.

4. Conclusions and outlook

We have outlined a laser power correction for LIF thermometry using a color camera. Our method exploits the different sensitivity of the red and green channels achieved by doping a RuPhen solution with a second dye, i.e. fluorescein or Riboflavin. We demonstrate the feasibility in a controlled

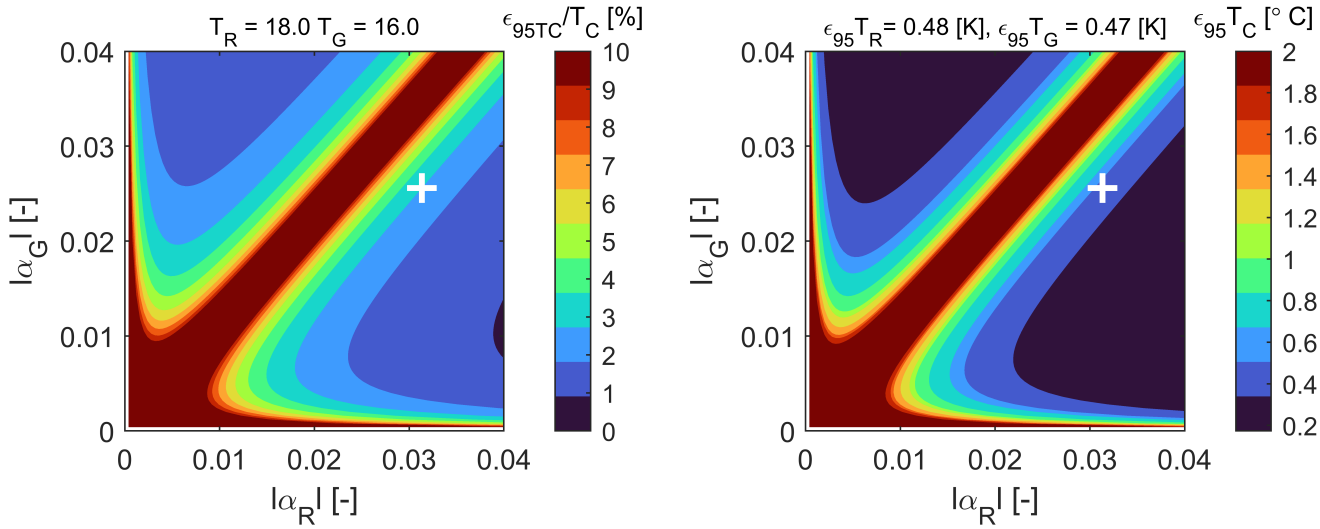

Figure 13. Maps of relative (left) and absolute (right) error at various combinations of β_R and β_G for an average over 20 exposures. In this case $\delta T_R = 0.1°C$ and $\delta T_G = 0.05°C$, while T_R and T_G are equal to 18 and 17.5 $°C$, respectively.

setup, where calibration data can be obtained using samples at a precisely controlled temperature. We model the relationship between the normalized image intensity and the sample temperature with a single or a double exponential model, finding that the latter allows for a more robust correction of the laser power fluctuations. The method compares also favourably to classical ratiometric approaches, which can lead to a deterioration of the temperature sensitivity. Based on our promising results, we plan to perform a large scale experiment to demonstrate the capability of our method. Our method can be extended to increase the precision and accuracy of other intensity based measurement techniques, such as, for example, binary pressure sensitive paints.

Acknowledgements

We would like to thank Stephan Kunz and Roger Vonbank, for their support at Empa for the experimental setup. Finally, we thank Dr. Hossein Gorji for fruitful discussions.

References

Barigozzi, G., Mucignat, C., Abdeh, H., Scandella, D., & Dolci, G. (2018). Assessment of binary PSP technique for film cooling effectiveness measurement on nozzle vane cascade with cutback trailing edge. *Experimental Thermal and Fluid Science*, *97*(December 2017), 431–443. Retrieved from `https://doi.org/10.1016/j.expthermflusci.2018.05.015` doi:

Coppeta, J., & Rogers, C. (1998). Dual emission laser induced fluorescence for direct planar scalar behavior measurements. *Experiments in Fluids*, *25*, 1-15. doi:

Fujisawa, N., Funatani, S., & Katoh, N. (2005). Scanning liquid-crystal thermometry and stereo velocimetry for simultaneous three-dimensional measurement of temperature and velocity field in a turbulent Rayleigh-Bérnard convection. *Experiments in Fluids*, *38*(3), 291–303. doi:

Funatani, S., Fujisawa, N., & Ikeda, H. (2004). Simultaneous measurement of temperature and velocity using two-colour LIF combined with PIV with a colour ccd camera and its application to the turbulent buoyant plume. *Measurement Science and Technology*, *15*(5), 983. doi:

Lam, H., Kostov, Y., Tolosa, L., Falk, S., & Rao, G. (2012). A high-resolution non-contact fluorescence-based temperature sensor for neonatal care. *Measurement Science and Technology*, *23*(3), 035104. doi:

Lavieille, P., Lemoine, F., Lavergne, G., Virepinte, J. F., & Lebouché, M. (2000). Temperature measurements on droplets in monodisperse stream using laser-induced fluorescence. *Experiments in Fluids*, *29*(5), 429–437. doi:

Rochlitz, H., & Scholz, P. (2018). Application of laser-induced fluorescence technique in a duct flow with one heated wall. *Experiments in Fluids*, *59*(3), 1–20. Retrieved from `http://dx.doi.org/10.1007/s00348-018-2508-1` doi:

Shah, J., Allegrini, J., & Carmeliet, J. (2018). Ratiometric-2dye-LIF using non-toxic dyes for temperature measurements in large-scale water tunnels. In *Proceedings of the 19th international symposium on application of laser and imaging techniques to fluid mechanics. lisbon, portugal.* (ISBN: 978-989-20-9177-8)

Shah, J., Mucignat, C., Lunati, I., & Rösgen, T. (2024). Simultaneous PIV – LIF measurements using RuPhen and a color camera. *Experiments in Fluids*. Retrieved from `https://doi.org/10.1007/s00348-023-03742-4` doi:

Tagawa, M., Nagaya, S., & Ohta, Y. (2001). Simultaneous measurement of velocity and temperature in high-temperature turbulent flows: A combination of LDV and a three-wire temperature probe. *Experiments in Fluids*, *30*(2), 143–152. doi:

Tellinghuisen, J. (2020). Least Squares Methods for Treating Problems with Uncertainty in x and y. *Analytical Chemistry*, *92*(16), 10863–10871. doi:

Walker, D. A. (1987). A fluorescence technique for measurement of concentration in mixing liquids. *J. Phys. E: Sci. Instrum*, *20*. doi:

Yarin, Foss, & Tropea. (2007). *Handbook of Experimental Fluid Dynamics* (Springer, Ed.).

Zähringer, K. (2014). The use of vitamins as tracer dyes for laser-induced fluorescence in liquid flow applications. *Experiments in Fluids*, *55*. doi: